

Mirror modes: Nonmaxwellian distributions

M. Gedalin and Yu. E. Lyubarsky
Ben-Gurion University, Beer-Sheva 84105, Israel

M. Balikhin
ACSE, University of Sheffield, Mappin Street, Sheffield S1 3JD, United Kingdom

R.J. Strangeway and C.T. Russell
IGPP/UCLA, 405 Hilgard Ave., Los Angeles, CA 90095-1567
(Dated: October 24, 2018)

We perform direct analysis of mirror mode instabilities from the general dielectric tensor for several model distributions, in the longwavelength limit. The growth rate at the instability threshold depends on the derivative of the distribution for zero parallel energy. The maximum growth rate is always $\sim k_{\parallel} v_{T\parallel}$ and the instability is of nonresonant kind. The instability growth rate and its dependence on the propagation angle depend on the shape of the ion and electron distribution functions.

PACS numbers:

I. INTRODUCTION

Numerous observations of waves in the the Earth magnetosheath, as well as at other planets have stimulated studies of long-wavelength and low-frequency modes in high β magnetized plasmas. It has been theoretically shown that the features of low-frequency waves in hot plasmas differ significantly from those in cool plasmas, even in the limit corresponding to the usual magnetohydrodynamic waves [1]. These findings have been subsequently proven by direct comparison with observations [2]. However, particular interest to the low-frequency modes in hot plasmas is explained by observations of the mirror modes, which were found in planetary magnetosheaths [3, 4, 5, 6], in the solar wind [7], in cometary comas [8, 9], and in the wake of Io [10, 11]. These modes are nonpropagating zero frequency modes (sometimes considered as the kinetic counterpart of the hydrodynamical entropy mode), which are expected to grow in an anisotropic plasma with sufficiently high $\beta_{\perp}/\beta_{\parallel}$ (see, e.g., Hasegawa [12]).

Usual high amplitudes of observed mirror modes show that they easily achieve the nonlinear regime. At the same time, in several cases low-amplitude magnetic field structures with the same properties were observed which may mean that the linear and nonlinear mirror mode features are generically related. Yet we do not know so far what makes these modes so ubiquitous and what determines their nonlinear amplitudes.

The early explanation of the mirror instability [12] is based on the simple picture of the adiabatic response of the anisotropic pressure of magnetized particles. Numerical analyses of the mirror instability in bi-Maxwellian plasmas [13, 14, 15] have shown that the maximum of the growth rate occurs at $k_{\perp}\rho_i \sim 1$ (where ρ_i is the ion thermal gyroradius), which was interpreted as an indication on the kinetic nature of the instability.

At the same time, Southwood and Kivelson [16] proposed a new explanation of the instability mechanism as a resonant one, where the presence of a group of the resonant particles (with $v_{\parallel} = 0$) plays the *destructive* role in the mode excitation: the growth rate of the instability is claimed to be inversely proportional to the number of the resonant particles. This explanation was further reiterated with some modifications by Pantellini and Schwartz [17] and Pokhotelov et al. [18], and used by Kivelson and Southwood [19] for the explanation of the nonlinear saturation mechanism. The analysis of Southwood and Kivelson [16] is done in the regime where the phase velocity of the perturbation is much less than the parallel thermal velocity, in other words, $\gamma \ll k_{\parallel} v_{T_i\parallel}$, and therefore, is directly applied only at the very threshold of the instability. At the same time, numerical calculations [15] show that most important events occur in the range $\gamma \sim k_{\parallel} v_{T_i\parallel}$, which is not covered in the previous analytical studies.

The previous analytical and numerical considerations of the linear regime of the mirror instability, even in the longwavelength limit, are, as a rule, restricted to the usage of the bi-Maxwellian distribution. At the same time particle distributions in collisionless plasma may substantially differ from the Maxwellian. For example, due to the ion heating mechanism at the shock (see, e.g., Skopke et al. [20]), the magnetosheath ion distributions may well deviate from the bi-Maxwellian. It is therefore of interest to study the dependence of the instability on the shape of the ion and electron distributions.

Yet another argument in favor of the analysis of other distributions is that there is no good analytical approximations for the dielectric tensor for the Maxwellian plasma in the range $|\omega|/k_{\parallel} v_{T\parallel} \sim 1$, which forced researchers to consider more convenient asymptotics. It is, however, possible to find the shapes of the distribution which allow closed analytical presentation of the dielectric tensor in the whole range of phase velocities and make the study of the instability physics more transparent.

In the present paper we study in detail the dependence of the mirror instability on the shape of the ion and electron distributions, using model distribution functions which allow direct explicit analytical calculation of the dielectric tensor. We establish the

generic relation of the mirror instability with the oscillatory modes when the Landau damping is absent and study the transition of damping modes to the unstable regime. We also propose an approximation which is useful for the analytical treatment of the instability in the most important range $\gamma \sim k_{\parallel} v_{T_{i\parallel}}$ in general case.

The paper is organized as follows. In section II we derive the general dispersion relation in the longwavelength for arbitrary distribution function. In sections III-IV we apply the general analysis to three different distributions. In section V we derive the instability condition and the growth rate at the threshold for arbitrary distribution. In section VI we develop a useful approximation for the analysis of the bi-Maxwellian-kind distributions in the region of the maximum growth rate.

II. DISPERSION RELATION IN THE LONGWAVELENGTH LIMIT

In what follows we will be interested in the longwavelength limit where $\omega \ll \Omega$ and $kv_T \ll \Omega$, while maintaining the phase velocity finite $0 < \omega/k < \infty$. The last inequality means that the phase velocity does not tend to zero in all propagation angle range but it certainly may vanish for particular set of parameters. For simplicity we assume that both ions and electrons are Maxwellian in the perpendicular direction, so that $\langle v_{\perp}^2 \rangle = 2v_{T\perp}^2$ and $\langle v_{\perp}^4 \rangle = 8v_{T\perp}^4$. We also denote $\langle v_{\parallel}^2 \rangle = v_{T\parallel}^2$ and $\beta_{\parallel,\perp} = 2v_{T\parallel,\perp}^2 \omega_p^2 / c^2 \Omega^2$ for each species (subscript i stands for ions and subscript e for electrons). Let us introduce the refraction index vector $\mathbf{N} = \mathbf{k}c/\omega$, such that $\mathbf{N} = (N_{\perp}, 0, N_{\parallel}) = N(\sin \theta, 0, \cos \theta)$. With all this the components of the dispersion matrix $D_{ij} = N^2 \delta_{ij} - N_i N_j - \epsilon_{ij}$ take the following form (see Appendix B):

$$D_{11} = N_{\parallel}^2 \left(1 - \frac{1}{2}(\beta_{\parallel} - \beta_{\perp})\right) - 1 - \frac{\omega_{pi}^2}{\Omega_i^2} - \frac{\omega_{pe}^2}{\Omega_e^2}, \quad (1)$$

$$D_{12} = 0, \quad (2)$$

$$D_{13} = -N_{\parallel} N_{\perp} \left(1 - \frac{1}{2}(\beta_{\parallel} - \beta_{\perp})\right), \quad (3)$$

$$D_{22} = N^2 \left(1 - \frac{1}{2} \cos^2 \theta (\beta_{\parallel} - \beta_{\perp}) + \sin^2 \theta \beta_{\perp}\right. \quad (4)$$

$$\left. - \sin^2 \theta (r_i \beta_{i\perp} \bar{\chi}_i + r_e \beta_{e\perp} \bar{\chi}_e)\right) - 1 - \frac{\omega_{pi}^2}{\Omega_i^2} - \frac{\omega_{pe}^2}{\Omega_e^2},$$

$$D_{23} = -i \frac{\omega_{pi}^2 \tan \theta}{\Omega_i \omega} (r_i \bar{\chi}_i - r_e \bar{\chi}_e), \quad (5)$$

$$D_{33} = N_{\perp}^2 \left(1 - \frac{1}{2}(\beta_{\parallel} - \beta_{\perp})\right) - 1 - \frac{\omega_{pi}^2 \beta_{i\parallel}}{k_{\parallel}^2 v_{T_{i\parallel}}^2} \left(\frac{\bar{\chi}_i}{\beta_{i\parallel}} + \frac{\bar{\chi}_e}{\beta_{e\parallel}}\right) \quad (6)$$

$$+ \frac{\omega_{pi}^2 \tan^2 \theta}{\Omega_i^2} r_i \bar{\chi}_i + \frac{\omega_{pe}^2 \tan^2 \theta}{\Omega_e^2} r_e \bar{\chi}_e,$$

where $\beta_{\parallel} = \beta_{i\parallel} + \beta_{e\parallel}$, $\beta_{\perp} = \beta_{i\perp} + \beta_{e\perp}$, $r_i = \beta_{i\perp} / \beta_{i\parallel}$, $r_e = \beta_{e\perp} / \beta_{e\parallel}$, and

$$\bar{\chi} = v_{T\parallel}^2 \int (u - v_{\parallel})^{-1} \frac{\partial f}{\partial v_{\parallel}} dv_{\parallel}. \quad (7)$$

The integration in (7) is taken along the path below the singularity $v_{\parallel} = u$. In what follows we shall also assume that $\omega_{pi}^2 / \Omega_i^2 \gg 1$ and neglect unity relative to this large parameter (which corresponds to the assumption $v_A \ll c$, where $v_A = c\Omega_i / \omega_{pi}$ is the Alfvén velocity). In what follows we also neglect $\omega_{pe}^2 / \Omega_e^2 = (\omega_{pi}^2 / \Omega_i^2)(m_e / m_i)$. In the above derivation we used $\omega_{pi}^2 / \Omega_i = -\omega_{pe}^2 / \Omega_e$ in the quasineutral electron proton plasma (this is not correct if any admixture of other charged particles is present).

In the limit $\omega / \Omega_i \rightarrow 0$ (and ω / k finite) the dispersion relation $D = \det \|D_{ij}\| = 0$ splits into two ones. One describes the purely transverse Alfvén wave (the wave electric field vector in the \mathbf{kB}_0 plane, the wave magnetic field vector perpendicular to the external magnetic field) with the dispersion

$$\omega_2 = k^2 v_A^2 \cos^2 \theta \left(1 - \frac{1}{2}(\beta_{\parallel} - \beta_{\perp})\right). \quad (8)$$

In this wave the absolute value of the magnetic field does not change, but the magnetic field rotates.

The second dispersion relation reads

$$\Psi(Z) = \left[2 - \cos^2 \theta (\beta_{\parallel} - \beta_{\perp}) + 2 \sin^2 \theta \beta_{\perp} - 2 \sin^2 \theta (r_i \beta_{i\perp} \bar{\chi}_i + r_e \beta_{e\perp} \bar{\chi}_e)\right. \quad (9)$$

$$\left. - Z^2 \beta_{i\parallel} \cos^2 \theta \right] \left[\frac{\bar{\chi}_i}{\beta_{i\parallel}} + \frac{\bar{\chi}_e}{\beta_{e\parallel}}\right] + \sin^2 \theta [r_i \bar{\chi}_i - r_e \bar{\chi}_e]^2 = 0,$$

where we introduced $Z = \omega/k_{\parallel}v_{T_{i\parallel}}$ for convenience (ω is complex, in general, so that $Z = W + iG$), and $r_{i,e} = \beta_{i,e\perp}/\beta_{i,e\parallel}$. Eq. (9) describes elliptically polarized waves with all three components of the wave electric field present, so that in general there exists a nonzero component of the wave magnetic field $B_z = N_{\perp}E_y$ in the direction of the external magnetic field. These waves not only rotate the magnetic field but change its magnitude as well.

The functions $\bar{\chi}$ play the crucial role in the subsequent analysis. They are defined by the integral containing the distribution function $f(v_{\parallel})$ and cannot be explicitly calculated without particular choice of these distributions. It is common to choose f as Maxwellian. In this case $\bar{\chi}$ is well-known and tabulated but has good asymptotic expansions only for $|Z| \ll 1$ or $|Z| \gg 1$ (for electrons Z should be substituted by $Z(m_e/m_i)(v_{T_{i\parallel}}/v_{T_{e\parallel}})$). This actually restricts possible analytical considerations of the mirror instability only with the range $|Z| \ll 1$. Yet, numerical analyses show that the most important events occur in the vicinity of $|Z| \sim 1$ which is unavailable to direct theoretical analysis when Maxwellian is chosen. On the other hand, there are vague indications that the qualitative features of long waves (instabilities) in the high β more or less sensibly depend on the lowest moments of the distribution function (provided it is sufficiently “normal”: smooth, no beams, no holes, etc.). It therefore makes sense to investigate the dispersion relations for a suitably chosen model distribution so that $\bar{\chi}$ can be calculated and analyzed in the range $|Z| \sim 1$. In what follows we shall use three different distributions for these purposes. The waterbag distribution $f = \Theta(v_0^2 - v_{\parallel}^2)/2v_0$ will be used for study of the behavior of longwavelength modes and their dependence on the plasma parameters in the absence of Landau damping. Here $\Theta(x) = 1$ if $x > 0$ and $\Theta(x) = 0$ if $x < 0$. The hard-bell distribution $f = 3(v_0^2 - v_{\parallel}^2)\Theta(v_0^2 - v_{\parallel}^2)/4v_0^3$ will allow to include the Landau damping effects, and the Lorentz-like distribution $f = (2v_0^3/\pi)(v_0^2 + v_{\parallel}^2)^{-2}$ removes the upper limit on the particle velocities. The four distributions (including Maxwellian $f = (2\pi v_{T_{\parallel}}^2)^{-1/2} \exp(-v_{\parallel}^2/2v_{T_{\parallel}}^2)$) mentioned in this paper are shown in Figure 1.

III. WATERBAG

The waterbag distribution $f = \Theta(v_0^2 - v_{\parallel}^2)/2v_0$ is somewhat peculiar since the Landau damping is absent. The analysis of this distribution allows to establish the generic relation of the instability to nondamping propagating modes. It is easy to find that in this case

$$\bar{\chi}_i = \frac{1}{3 - Z^2}, \quad \bar{\chi}_e = \frac{1}{3 - Z^2\mu R} \quad (10)$$

where $\mu = m_e/m_i \approx 1/2000$, $R = \beta_{i\parallel}/\beta_{e\parallel}$, and $v_{T_{\parallel}}^2 = v_0^2/3$. In the limit $Z = 0$ one has $d \equiv \bar{\chi}(Z = 0) = 1/3$. It is worth noting that for the Maxwellian distribution $d = 1$. In this section we use for electrons the approximation of the massless bi-Maxwellian (instead of above waterbag, which is used only for ions), for which $\bar{\chi}_e = 1$. The resulting dispersion relation (9) is a third order equation with respect to Z^2 with real coefficients. Although this equation can be analyzed directly and even solved analytically, graphical representation of the roots is much more convenient.

Figure 2 shows the mode with the highest phase velocity (fast mode) for the case when $\beta_{i\parallel} = \beta_{i\perp} = \beta_{e\parallel} = \beta_{e\perp} = 0.1$ and massless bi-Maxwellian electrons. It is worth noting that ions are *not* isotropic since they are Maxwellian in the perpendicular direction and waterbag in the parallel direction. The phase velocity of the fast mode is well above $k_{\parallel}v_{T_{i\parallel}}$ so that it has nothing to do with the mirror instability. We do not consider this mode in the rest of the paper. We do not consider the Alfvén mode either. The remaining two low-phase velocity modes are shown in Figure 3 together with $\omega = k_{\parallel}v_{0i}$ (solid line). The upper curve is above the resonant region having $|\omega| > |k_{\parallel}v_{\parallel}|$ for all ions. The lower mode is inside the resonant region and would damp if there were nonzero $\partial f/\partial v_{\parallel}$.

Figure 4 shows the same two modes but in the case $\beta_{i\parallel} = \beta_{i\perp} = \beta_{e\parallel} = \beta_{e\perp} = 0.5$. In both cases the naive instability condition

$$K = \beta_{\perp}/\beta_{\parallel} - 2 - 2/\beta_{\perp} > 0 \quad (11)$$

is not fulfilled, although in the second case K is closer to the threshold just because of the larger β_{\perp} . There is no much difference in the behavior of the two modes for these two cases, except a little stronger decrease of the phase velocities towards the perpendicular propagation regime in the higher β_{\perp} case.

Figure 5 shows the behavior of the two modes in the anisotropic case $\beta_{i\parallel} = \beta_{e\parallel} = 0.1$, $\beta_{i\perp} = \beta_{e\perp} = 0.5$ (so that $K = 1$), and bi-Maxwellian electrons. The lower mode now remains purely propagating mode for smaller angles (diamonds) but turns into an aperiodic instability for larger angles of propagation (stars). The obvious conclusion from Figure 5 is that the unstable mode has its propagation counterpart for the smaller angles of propagation. The relative growth rate $G = \gamma/k_{\parallel}v_{T_{i\parallel}} \sim 1$ is large in the whole range of instability, so that the approximation $G \ll 1$ [16] is not applicable.

It is of interest to compare this case with the massless waterbag electrons $\bar{\chi}_e = 1/3$. The corresponding curves in Figure 6 show that there is no instability in this case despite the fact that the threshold (11) is exceeded.

Thus, the analysis of the waterbag distribution already shows that (a) there is, in general, the propagating counterpart of the mirror instability if Landau damping is absent, (b) the instability threshold and growth rate are sensitive to the details of the

distribution and not only to the second moment, and (c) the instability is aperiodic, that is, in the unstable range $W = 0$ and $G > 0$. It can be shown that the last feature is generally valid unless the distribution function is very peculiar (see Appendix C).

IV. HARD-BELL AND LORENTZ DISTRIBUTIONS

The waterbag distribution does not allow Landau damping since $\partial f / \partial v_{\parallel} = 0$ everywhere. In order to get rid of this restriction we consider the hard-bell distribution $f = 3(v_0^2 - v_{\parallel}^2)\Theta(v_0^2 - v_{\parallel}^2)/4v_0^3$, which has nonzero derivative but is compact ($f = 0$ for $|v_{\parallel}| > v_0$). In this case

$$\bar{\chi}_i = \frac{3}{5} \left[1 + \frac{Z}{4\sqrt{5}} \ln \frac{(\sqrt{5} - W)^2 + G^2}{(\sqrt{5} + W)^2 + G^2} + \frac{iZ}{2\sqrt{5}} \left(\arctan \frac{\sqrt{5} - W}{G} + \arctan \frac{\sqrt{5} + W}{G} \right) \right], \quad (12)$$

where $Z = W + iG$, W and G being real, $G > 0$, and $v_0^2 = 5v_{T\parallel}^2$. The corresponding $d = \bar{\chi}(Z = 0) = 3/5$. The corresponding expression for $\bar{\chi}_e$ is obtained from (12) by substitution $Z \rightarrow Z\sqrt{\mu R}$.

In order to analyze non-compact distributions too we shall consider the Lorentz distribution $f = (2v_0^3/\pi)(v_0^2 + v_{\parallel}^2)^{-2}$. In this case

$$\bar{\chi}_i = \frac{16iZ}{(1 + Z^2)^3} + \frac{3i}{i - Z} - \frac{2Z}{(i - Z)^3} + \frac{3iZ}{(i - Z)^2}, \quad (13)$$

with $v_0^2 = v_{T\parallel}^2$ and $d = 3$. Again, $\bar{\chi}_e$ is obtained by substitution $Z \rightarrow Z\sqrt{\mu R}$.

We shall also compare the results for these distributions with the bi-Maxwellian. In this case there is no compact analytical expression for χ and we use direct numerical calculation.

In what follows we are interested only in the unstable region. The subparticle mode is expected to be strongly damped in the propagation range. The ‘‘superparticle’’ mode is not damped in the hard-bell case and almost not damped in the Lorentz case.

As the first set of parameters for the unstable regime we choose $\beta_{i\parallel} = \beta_{e\parallel} = 0.1$, $\beta_{i\perp} = \beta_{e\perp} = 0.5$, and massless bi-Maxwellian electrons $\bar{\chi}_e = 1$. Figure 7 shows the growth rates for the three distributions. The highest growth rate is for the Lorentzian, the lowest is for the waterbag. Figure 8 shows the same growth rates as in Figure 7 but normalized on $kv_{Ti\parallel}$ which allows to compare growth rates of the modes with the same wavenumber k and different angles of propagation. It is seen that the maximum growth rates is achieved approximately at the same angle of propagation $\approx 60^\circ$ for all distributions, but the threshold angle moves towards more quasiparallel regimes for distributions with stronger tails (Maxwellian and Lorentzian).

Figure 9 shows the dependence of the growth rate on β_{\perp} when $K = 1$ and $\beta_{i\perp}/\beta_{e\parallel} = \beta_{i\parallel}/\beta_{e\parallel} = 1$ remain constant. Both curves correspond to the waterbag ions and massless bi-Maxwellian electrons. Diamonds stand for the same parameters as in Figure 5, crosses correspond to $\beta_{i\perp} = 1$ and $\beta_{i\parallel} = 0.25$. The instability is stronger for higher β_{\perp} .

In the previous analysis we always used the approximation of massless bi-Maxwellian distribution corresponding to $\chi_e = 1$. Figures 10 and 11 show the growth rate of the instability when the electron distributions are chosen in the same form as the ion distributions. One can see that the waterbag distributions become stable, while the growth rate in the case of Lorentzian drastically increases. The ratio of the maximum growth rates shown in Figures 8 and 11 roughly corresponds to $d_e = \chi_e(Z = 0)$ which shows that the maximum growth rate significantly on electrons (see sections V and VI).

For other combinations of ion and electron distributions the ratios may be even greater as is seen in Figure 12, where diamonds correspond to waterbag ions and massless bi-Maxwellian electrons, while circles correspond to waterbag ions and Lorentz electrons. The β parameters are the same for both cases.

V. NEAR THE THRESHOLD

It is possible to obtain general results just above the threshold of the instability, where $Z = iG \rightarrow +0$. For $f = f(v^2)$ it is easy to find

$$\begin{aligned} \chi &= \int \frac{1}{iG - v_{\parallel}} \frac{\partial f}{\partial v_{\parallel}} dv_{\parallel} \\ &= - \int \frac{v_{\parallel}}{v_{\parallel}^2 + G^2} \frac{\partial f}{\partial v_{\parallel}} dv_{\parallel} = - \int \frac{df}{d\mathcal{E}} dv_{\parallel} + G \int \frac{G}{v_{\parallel}^2 + G^2} \frac{df}{d\mathcal{E}} dv_{\parallel} \\ &= - \int \frac{df}{d\mathcal{E}} dv_{\parallel} + \pi G \frac{df}{d\mathcal{E}} \Big|_{v_{\parallel}=0} = d - \kappa G, \end{aligned} \quad (14)$$

where $\mathcal{E} = v_{\parallel}^2/2$ is the energy (on the unit mass). Substituting this into (9) and neglecting all terms of the order Z^2 and higher, one has

$$G = -A/B, \quad (15)$$

$$A = [2 - \cos^2 \theta (\beta_{\parallel} - \beta_{\perp}) + 2 \sin^2 \theta \beta_{\perp} - 2 \sin^2 \theta (r_i \beta_{i\perp} d_i + r_e \beta_{e\perp} d_e)] \left(\frac{d_i}{\beta_{i\parallel}} + \frac{d_e}{\beta_{e\parallel}} \right) + \sin^2 \theta (r_i d_i - r_e d_e)^2, \quad (16)$$

$$B = -\frac{\kappa_i}{\beta_{i\parallel}} [2 - \cos^2 \theta (\beta_{\parallel} - \beta_{\perp}) + 2 \sin^2 \theta \beta_{\perp} - 2 \sin^2 \theta (r_i \beta_{i\perp} d_i + r_e \beta_{e\perp} d_e)] + 2 \sin^2 \theta r_i \beta_{i\perp} \kappa_i \left(\frac{d_i}{\beta_{i\parallel}} + \frac{d_e}{\beta_{e\parallel}} \right) - 2 \sin^2 \theta \kappa_i (r_i d_i - r_e d_e), \quad (17)$$

where we neglected $\kappa_e \sim \kappa_i \sqrt{m_e/m_i}$. The instability threshold for given θ is found from the condition $G = 0$, that is, $A = 0$, which gives

$$2 + \beta_{\perp} - \beta_{\parallel} + \sin^2 \theta [\beta_{\parallel} + \beta_{\perp} - 2(r_i \beta_{i\perp} d_i + r_e \beta_{e\perp} d_e) + (r_i d_i - r_e d_e)^2 / (d_i / \beta_{i\parallel} + d_e / \beta_{e\parallel})] = 0. \quad (18)$$

Since $0 \leq \sin^2 \theta \leq 1$, the global instability criterion reads (in the assumption that $2 + \beta_{\perp} > \beta_{\parallel}$):

$$2(r_i \beta_{i\perp} d_i + r_e \beta_{e\perp} d_e) - 2 - 2\beta_{\perp} - (r_i d_i - r_e d_e)^2 \left(\frac{d_i}{\beta_{i\parallel}} + \frac{d_e}{\beta_{e\parallel}} \right)^{-1} > 0. \quad (19)$$

It is instructive to consider several simple cases. We can neglect completely the electron contribution by putting $d_e = 0$, which gives the instability criterion in the form

$$\frac{d\beta_{\perp}}{\beta_{\parallel}} > 2 \left(1 + \frac{1}{\beta_{\perp}} \right), \quad (20)$$

and for the bi-Maxwellian distribution, $d = 1$, reduces to the naive mirror instability criterion.

On the other hand, when $r_e = r_i = \beta_{\perp}/\beta_{\parallel}$ and $d_e = d_i = d$, one gets

$$\frac{d\beta_{\perp}}{\beta_{\parallel}} > 1 + \frac{1}{\beta_{\perp}}. \quad (21)$$

This condition is harder for more compact distributions ($d = 1/3$ for waterbag and $d = 3/5$ for hard-bell) and softer for distributions with long tails ($d = 1$ for Maxwellian and $d = 3$ for Lorentzian). The global instability condition (19) can be written in a more symmetric form as follows:

$$(r_i d_i + r_e d_e)^2 + \frac{2(\beta_{i\perp}^2 + \beta_{e\perp}^2) d_e d_i}{\beta_{i\parallel} \beta_{e\parallel}} - 2(1 + \beta_{\perp}) \left(\frac{d_e}{\beta_{e\parallel}} + \frac{d_i}{\beta_{i\parallel}} \right) > 0 \quad (22)$$

which emphasizes the symmetric role of ions and electrons in the instability onset (cf. Pokhotelov et al. [18]).

Indeed, near the threshold $\gamma/k_{\parallel} v_{T\parallel} \ll 1$ and the response of both electrons and ions is adiabatic, that is, their inertia does not play any role. In these circumstances the mass of the particle is of not importance. Their role in the response to the parallel electric field is, however, antisymmetric because of the different signs of the charge: the adiabatic response is obtained from $eE_z - (1/n)(dp/dz) = eE_z - ik_{\parallel} p/n = 0$. The parallel response plays the crucial role in the instability development. As is known the instability occurs because of the breakdown of the local frozen-in condition and efficient drag of particles out of the field enhancement into the field depletion region [16, 17, 18]. Thus, when the magnetic field is perturbed, $B_z = B_0 + \delta B_z$, the perturbation of the density of the species s is

$$\frac{\delta n_s}{n_{0s}} = \frac{\delta B_z}{B_0} + \frac{\delta n_s^{(\text{ext})}}{n_{0s}}, \quad (23)$$

where $\delta n_s^{(\text{ext})}$ is due to the motion along the field lines. In the adiabatic regime $\gamma/k_{\parallel} v_{T\parallel} \ll 1$ this change can be considered as a quasistatic response to the effective potential $\phi_{\text{eff}} = \phi + \mu_s \delta B_z / q_s$, where ϕ is the electrostatic potential, $\mu_s = \langle v_{\perp}^2 \rangle_s / 2B_0$ is

the average magnetic moment, and q_s is the charge of the species. The density response to this effective potential can be found from the reduced Vlasov equation

$$\frac{\partial f_s}{\partial t} + v_{\parallel} \frac{\partial f_s}{\partial z} = q_s \frac{\partial \phi_{\text{eff}}}{\partial z} \frac{\partial f_s}{\partial v_{\parallel}}, \quad (24)$$

which for $\partial/\partial t = \gamma$ and $\partial/\partial z = ik_{\parallel}$ gives

$$\frac{\delta n_s^{(\text{ext})}}{n_{0s}} = \phi_{\text{eff}} \int \frac{ik_{\parallel}}{\gamma + ik_{\parallel}v_{\parallel}} \frac{\partial f_s}{\partial v_{\parallel}} dv_{\parallel}. \quad (25)$$

It is easy to see that in the adiabatic regime near the threshold of the instability, $\gamma \rightarrow 0$, this expression reduces to the following

$$\frac{\delta n_s^{(\text{ext})}}{n_{0s}} = -\frac{q_s \phi_{\text{eff}}}{4\pi n_{0s} q_s^2 r_D^2}, \quad (26)$$

where r_D is the Debye length calculated with the parallel distribution function. It is easy to see that $r_D^2 = v_{T\parallel}^2/\omega_p^2 d$, where $d = \bar{\chi}(Z = 0)$. The electrostatic potential ϕ can be excluded using the quasineutrality condition $\delta n_e = \delta n_i$, which eventually gives

$$\frac{\delta n}{n} = \frac{\delta B_z}{B_0} \left[1 - \frac{T_{e\perp} + T_{i\perp}}{4\pi e^2 n_0 (r_{De}^2 + r_{Di}^2)} \right], \quad (27)$$

where we have taken into account that $\mu = T_{\perp}/B_0$. Eq. (27) shows that smaller Debye lengths r_D (larger d) result in the stronger drag of the particles into the weak field region, that reducing the kinetic pressure response to the magnetic field enhancement and supporting instability. Therefore, stronger Debye screening (larger d) would lower the instability threshold, in agreement with the found from rigorous calculations.

From (15)–(17) it is easily seen that the growth rate is inversely proportional to $\kappa_i = -\pi(df/d\mathcal{E})|_{v_{\parallel}=0}$, and not to the number of particles with $v_{\parallel} = 0$ (cf. Southwood and Kivelson [16]). The latter is correct for the bi-Maxwellian distribution since $(df/d\mathcal{E}) \propto f$ in this case. For other distributions this relation may well be wrong. For example, for the waterbag distribution $(df/d\mathcal{E})|_{v_{\parallel}=0} = 0$ and higher order terms should be retained to investigate the behavior near the threshold. It is easy to see from (14) that in this case $\bar{\chi} = d - \alpha G^2$, where $\alpha = -\int v_{\parallel}^{-2} (df/d\mathcal{E}) dv_{\parallel}$ is well-defined. The dispersion relation (9) becomes than a first order equation for G^2 , which has one positive solution near the threshold. It is clear that in this case the growth rate is determined by the whole distribution and not only by the behavior in $v_{\parallel} = 0$.

VI. HYDRODYNAMICAL REGIME

The previous analysis shows that maximum Z is always of the order of unity or larger, which means that ions no longer respond adiabatically to the magnetic field enhancements and their inertia begins to play an important role. This also means that it is thermal particles of the ion distribution body with $v \sim v_{T\parallel}$ which are mainly responsible for the instability development and not the group of resonant particles with $v_{\parallel} = 0$. Figure 10 shows that for some distributions the instability may be very fast so that the electron inertia should be taken into account.

The previous analysis gives a clue to the treatment of the instability in the range of maximum growth rates, where $G \gtrsim 1$. Let us assume that the distribution function is such that $v_{\parallel} f(v_{\parallel})$ has a sharp maximum at some $v_m \sim v_{T\parallel}$. An example of a distribution of this kind is the Maxwellian $f_i = (1/\sqrt{2\pi}v_{T\parallel}) \exp(-v_{\parallel}^2/2v_{T\parallel}^2)$ for which there was no good approximation for $\bar{\chi}$ in the range $|Z| \sim 1$ so far. For the aperiodic mirror instability with $Z = iG$, $G > 0$, one has

$$\bar{\chi} = \int \frac{1}{iG - v_{\parallel}} \frac{\partial f}{\partial v_{\parallel}} dv_{\parallel} = - \int \frac{1}{G^2 + v_{\parallel}^2} v_{\parallel} \frac{\partial f}{\partial v_{\parallel}} dv_{\parallel}. \quad (28)$$

For $v_m \sim 1 \lesssim G$ (v_m is normalized on $v_{T\parallel}$) the function $(G^2 + v_{\parallel}^2)^{-1}$ varies slowly in the vicinity of the maximum of $v_{\parallel}(\partial f/\partial v_{\parallel})$, so that one may approximate

$$\bar{\chi} = -\frac{1}{G^2 + v_m^2} \int v_{\parallel} \frac{\partial f}{\partial v_{\parallel}} dv_{\parallel} = \frac{1}{G^2 + v_m^2}. \quad (29)$$

Figure 13 shows the comparison of the numerically found $\bar{\chi}$ for the Maxwellian distribution ($v_m^2 = 2$) and $Z = iG$, $G > 0$ with the approximation (29). The approximation proves to be very good for $G \geq 1$ and is only by the factor 2 smaller at

$G \rightarrow 0$. Figure 14 shows similar comparison for Lorentzian. Now the maximum growth rate can be obtained by substituting $\bar{\chi}_i = 1/(G^2 + v_{mi}^2)$ in (9). If G is expected to be high, so that $G^2 R\mu \sim 1$, as it occurs for the Lorentzian $e - i$ distributions in Figure 10, the electron inertia should be also taken into account by substituting $\bar{\chi}_e = 1/(G^2 R\mu + v_{me}^2)$. If, however, the growth rates are relatively modest (as in other cases studied in the present paper), the electrons still respond adiabatically and $\bar{\chi}_e = d_e$. In the last case (9) turns into a third order equation with respect to G^2 . Finding the maximum growth rate from this equation is a technical problem. We shall stop for a while at the physical sense of the above approximation. The dependence of the maximum growth rate on v_m indicates that the particles with high velocities $v \sim v_{T\parallel}$ are taking part in the process. This is related to the dynamic redistribution (closely related to the dynamic Debye screening): if the potential changes quickly the low velocity particles do not have enough time to change their position and leave the field enhancements. This redistribution is described by the same Eq. (25) but now $\gamma/k_{\parallel}v_{T\parallel} \sim 1$. High velocity particles can leave these regions and reduce the kinetic pressure response but their contribution rapidly decreases with the velocity since their number decreases. The increase of redistribution efficiency and the decrease of the number of screeners with the velocity increase finds its manifestation in that the main contribution belongs to the particles at the maximum of $v_{\parallel}f(v_{\parallel})$. Since the redistribution plays the destabilizing role, it can be expected that the smaller is v_m the higher is the growth rate. This can be seen already from Figure 8 where the growth rate for Lorentzian ions, $v_m^2 = 0.5$, is larger than the growth rate for the Maxwellian, $v_m^2 = 2$ (with the same massless Maxwellian electrons). Figure 15 shows the comparison of the growth rates obtained with the proposed approximation for several $v_m^2 = 2$ (diamonds), 1.5 (crosses), 1 (triangles), 0.5 (circles), and massless Maxwellian electrons. The parameters chosen are $\beta_{i\perp} = \beta_{e\perp} = 0.5$, $\beta_{i\parallel} = \beta_{e\parallel}$. As expected the decrease of v_m results in the increase of the maximum growth rate.

Finally, Figure 16 shows the comparison of the growth rates obtained directly and with the above approximation for Maxwellian (diamonds and crosses) and Lorentzian (triangles and circles), for the same parameter set. The agreement is quite satisfactory.

VII. CONCLUSIONS

We have derived the most general dispersion relation for longwavelength modes in hot plasmas. We have derived the general mirror instability condition for arbitrary ion and electron distributions and growth rate of the instability near the threshold. The instability threshold depends not only on the plasma species β but also on another integral characteristic of the distribution function $d = \int v_{\parallel}^{-1}(\partial f/\partial v_{\parallel})dv_{\parallel}$ for both species. Larger d corresponds to smaller Debye length. Smaller Debye length, in turn, corresponds to stronger response of the density to the perturbations of the potential, which allows stronger density depletions in the regions of the magnetic field enhancements. Therefore, the kinetic pressure response to the magnetic pressure buildup weakens. Hence, the larger is d the lower is instability threshold. The near-the-threshold growth rate is inversely proportional to $\partial f/\partial \mathcal{E}$, where $\mathcal{E} = v_{\parallel}^2/2$ is the parallel energy.

The mirror instability is always aperiodic and $(\gamma/k_{\parallel}v_{T_i\parallel})_{\max} \sim 1$ (and sometimes substantially greater). Maximum growth rates are normally determined by v_{mi} such that $v_{\parallel}\partial f_i/\partial v_{\parallel}$ has a sharp maximum in $v_{\parallel} = v_{mi}$, and d_e (if the instability is very strong v_{me} takes the place of d_e). This is related to the dynamic redistribution in which the thermal particles participate. Growth rates are higher for distributions with tails and lower for compact distributions (those, for which $f = 0$ if $|v_{\parallel}| > v_0$, where v_0 is some upper limit). For noncompact distributions the maximum growth rate is larger for smaller v_m , which corresponds to the weaker dynamic screening of the parallel electric field. For the distributions analyzed in this paper the behavior of d and v_m correlates (d increases when v_m decreases) since all these are single-parameter distributions. For more general distributions the behavior of d_e and v_m may be uncorrelated. It is also worth noting that it not, in general, any specific group of particles which are responsible for the instability development. Compare, for example, two similar distributions (velocity normalized on the thermal velocity $v_{T\parallel}$): $f_1 = (2/\pi)(1 + v_{\parallel}^2)^{-2}$ with $d = 3$ and $v_m^2 = 0.5$, and $f_2 = (\sqrt{2}/\pi)(1 + v_{\parallel}^4)^{-1}$ with $d = 1$ and $v_m^2 = 1$. While the behavior of the two is similar for $v_{\parallel} = 0$ and $v_{\parallel} \rightarrow \infty$ (the only difference is the factor $\sqrt{2}$), the first one is expected to be more unstable because of the three times stronger Debye screening. At the same time the behavior of the second distribution near the threshold should be close to that of the Maxwellian, $d = 1$, despite the very different suprathermal tails and $(df/d\mathcal{E})|_{v_{\parallel}=0}$.

We have also proposed a useful approximation for the dielectric function in the range $G/k_{\parallel}v_{T_i\parallel} \gtrsim 1$ for distributions with sharp maxima of $v_{\parallel}(\partial f/\partial v_{\parallel})$ (Maxwellian as one of such distributions). This approximation proves to be quite satisfactory for Maxwellian type distributions and allows to study analytically the instability behavior in the maximum growth rate range.

Acknowledgments

Figures are made using Matlab.

APPENDIX A: GENERAL EXPRESSIONS

We start with the general expression for the dielectric tensor in the following form:

$$\epsilon_{ij} = \delta_{ij} + \sum \lambda_{ij}, \quad (\text{A1})$$

where the summation is on the species and

$$\lambda_{ij} = -\frac{\omega_p^2}{\omega^2} \delta_{ij} + \eta_{ij}. \quad (\text{A2})$$

The expression for η_{ij} is well-known (see, e.g., Hasegawa [12]):

$$\eta_{ij} = -\sum_n \frac{\omega_p^2}{\omega^2} \int v_\perp dv_\perp dv_\parallel \left(\frac{n\Omega}{v_\perp} \frac{\partial f_0}{\partial v_\perp} + k_\parallel \frac{\partial f_0}{\partial v_\parallel} \right) \frac{\Pi_{ij}}{n\Omega - \zeta}, \quad (\text{A3})$$

where $\zeta = \omega - k_\parallel v_\parallel$, and

$$\Pi_{ij} = \begin{pmatrix} (n^2\Omega^2/k_\perp^2)J_n^2 & i(v_\perp n\Omega/k_\perp)J_n J_n' & (v_\parallel n\Omega/k_\perp)J_n^2 \\ -i(v_\perp n\Omega/k_\perp)J_n J_n' & v_\perp^2 J_n'^2 & -iv_\perp v_\parallel J_n J_n' \\ (v_\parallel n\Omega/k_\perp)J_n^2 & iv_\perp v_\parallel J_n J_n' & v_\parallel^2 J_n^2 \end{pmatrix}. \quad (\text{A4})$$

Here $J_n = J_n(x)$, $x = k_\perp \rho = k_\perp v_\perp / \Omega$, and $J_n' = dJ_n/dx$.

For the analysis in the low-frequency range $\omega/\Omega \ll 1$ let us write

$$\eta_{ij} = \eta_{ij}^{(0)} + \eta_{ij}^{(n \neq 0)}, \quad (\text{A5})$$

and expand

$$\frac{1}{n\Omega - \zeta} = \frac{1}{n\Omega} \left(1 + \frac{\zeta}{n\Omega} + \frac{\zeta^2}{n^2\Omega^2} + \dots \right).$$

Let also $f_0 = f_1(v_\perp)f_2(v_\parallel^2)$, and denote $\langle \dots \rangle = \int (\dots) f dv_j$, where $j = \perp, \parallel$.

One has

$$\eta_{ij}^{(0)} = \frac{\omega_p^2}{\omega^2} \int v_\perp dv_\perp dv_\parallel \frac{k_\parallel}{\zeta} \frac{\partial f_0}{\partial v_\parallel} \times \begin{pmatrix} 0 & 0 & 0 \\ 0 & v_\perp^2 J_0'^2 & -iv_\perp v_\parallel J_0 J_0' \\ 0 & iv_\perp v_\parallel J_0 J_0' & v_\parallel^2 J_0^2 \end{pmatrix} \quad (\text{A6})$$

and

$$\begin{aligned} \eta_{ij}^{(n \neq 0)} &= -\sum_n \frac{\omega_p^2}{\omega^2} \int v_\perp dv_\perp dv_\parallel \left(\frac{1}{v_\perp} \frac{\partial f_0}{\partial v_\perp} + \frac{k_\parallel}{n\Omega} \frac{\partial f_0}{\partial v_\parallel} \right) \\ &\times \left(1 + \frac{\zeta}{n\Omega} + \frac{\zeta^2}{n^2\Omega^2} \right) \Pi_{ij}. \end{aligned} \quad (\text{A7})$$

Now, up to Ω^{-2} one obtains

$$\eta_{11}^{(n \neq 0)} = -\sum_n \frac{\omega_p^2}{\omega^2} \left[\langle J_n^2 \frac{\partial}{\partial v_\perp} \rangle \frac{n^2\Omega^2 + \omega^2 + k_\parallel^2 \langle v_\parallel^2 \rangle}{k_\perp^2} + \frac{k_\parallel^2}{k_\perp^2} \langle v_\perp J_n^2 \rangle \right], \quad (\text{A8})$$

$$\eta_{12}^{(n \neq 0)} = -i \sum_n \frac{\omega_p^2}{\omega^2} \frac{\omega}{k_\perp} \langle v_\perp J_n J_n' \frac{\partial}{\partial v_\perp} \rangle, \quad (\text{A9})$$

$$\eta_{13}^{(n \neq 0)} = \sum_n \frac{\omega_p^2}{\omega^2} \frac{k_\parallel}{k_\perp} \left[\langle v_\perp J_n^2 \rangle + \langle v_\parallel^2 \rangle \langle J_n^2 \frac{\partial}{\partial v_\perp} \rangle \right], \quad (\text{A10})$$

$$\eta_{22}^{(n \neq 0)} = -\sum_n \frac{\omega_p^2}{\omega^2} \left[\langle v_\perp^2 J_n'^2 \frac{\partial}{\partial v_\perp} \rangle \left(1 + \frac{\omega^2 + k_\parallel^2 \langle v_\parallel^2 \rangle}{n^2\Omega^2} \right) + \frac{k_\parallel^2}{n^2\Omega^2} \langle v_\perp^3 J_n'^2 \rangle \right], \quad (\text{A11})$$

$$\eta_{23}^{(n \neq 0)} = -i \sum_n \frac{\omega_p^2 k_{\parallel}}{\omega n^2 \Omega^2} \left[\langle v_{\perp}^2 J_n J'_n \rangle + 2 \langle v_{\parallel}^2 \rangle \langle v_{\perp} J_n J'_n \frac{\partial}{\partial v_{\perp}} \rangle \right], \quad (\text{A12})$$

$$\eta_{33}^{(n \neq 0)} = - \sum_n \frac{\omega_p^2}{\omega^2} \langle v_{\parallel}^2 \rangle \langle J_n^2 \frac{\partial}{\partial v_{\perp}} \rangle, \quad (\text{A13})$$

and

$$\eta_{22}^{(0)} = \frac{\omega_p^2}{\omega^2} k_{\parallel} \langle v_{\perp}^3 J_0'^2 \rangle \chi, \quad (\text{A14})$$

$$\eta_{23}^{(0)} = -i \frac{\omega_p^2}{\omega} \langle v_{\perp}^2 J_0 J_0' \rangle \chi, \quad (\text{A15})$$

$$\eta_{33}^{(0)} = \frac{\omega_p^2}{\omega^2} \langle v_{\perp} J_0^2 \rangle \left(1 + \frac{\omega^2}{k_{\parallel}} \chi \right). \quad (\text{A16})$$

where

$$\chi = \left\langle \frac{1}{\zeta} \frac{\partial}{\partial v_{\parallel}} \right\rangle. \quad (\text{A17})$$

Using in Eqs.(A8)-(A13) the following summation rules

$$\sum_{n \neq 0} J_n^2 = 1 - J_0^2, \quad (\text{A18})$$

$$\sum_{n \neq 0} n^2 J_n^2 = \frac{x^2}{2} = \frac{k_{\perp}^2 v_{\perp}^2}{2\Omega^2}, \quad (\text{A19})$$

$$\sum_{n \neq 0} J_n J'_n = -J_0 J_0', \quad (\text{A20})$$

$$\sum_{n \neq 0} J_n'^2 = \frac{1}{2} - J_0'^2, \quad (\text{A21})$$

one obtains eventually the following general expression for λ_{ij} in the limit of $\omega, k_{\parallel} v_{\parallel} \ll \Omega$ when expanded up to the second order in ζ/Ω :

$$\lambda_{11} = \frac{\omega_p^2}{k_{\perp}^2} \left(1 + \frac{k_{\parallel}^2 \langle v_{\parallel}^2 \rangle}{\omega^2} \right) \langle J_0^2 \frac{\partial}{\partial v_{\perp}} \rangle - \frac{\omega_p^2 k_{\parallel}^2}{\omega^2 k_{\perp}^2} \langle v_{\perp} (1 - J_0^2) \rangle, \quad (\text{A22})$$

$$\lambda_{12} = i \frac{\omega_p^2}{\omega k_{\perp}} \langle v_{\perp} J_0 J_0' \frac{\partial}{\partial v_{\perp}} \rangle, \quad (\text{A23})$$

$$\lambda_{13} = \frac{\omega_p^2 k_{\parallel}}{\omega^2 k_{\perp}} \left[\langle v_{\perp} (1 - J_0^2) \rangle - \langle v_{\parallel}^2 \rangle \langle J_0^2 \frac{\partial}{\partial v_{\perp}} \rangle \right], \quad (\text{A24})$$

$$\lambda_{22} = \frac{\omega_p^2}{\omega^2} \langle v_{\perp}^2 J_0'^2 \frac{\partial}{\partial v_{\perp}} \rangle - \frac{\omega_p^2}{\omega^2} \sum_n \left[\frac{\omega^2 + k_{\parallel}^2 \langle v_{\parallel}^2 \rangle}{n^2 \Omega^2} \langle v_{\perp}^2 J_n'^2 \frac{\partial}{\partial v_{\perp}} \rangle + \frac{k_{\parallel}^2}{n^2 \Omega^2} \langle v_{\perp}^3 J_n'^2 \rangle \right] + \frac{\omega_p^2}{\omega^2} k_{\parallel} \langle v_{\perp}^3 J_0'^2 \rangle \chi, \quad (\text{A25})$$

$$\lambda_{23} = -i \sum_n \frac{\omega_p^2 k_{\parallel}}{\omega n^2 \Omega^2} \left[\langle v_{\perp}^2 J_n J'_n \rangle + 2 \langle v_{\parallel}^2 \rangle \langle v_{\perp} J_n J'_n \frac{\partial}{\partial v_{\perp}} \rangle \right] - i \frac{\omega_p^2}{\omega} \langle v_{\perp}^2 J_0 J_0' \rangle \chi, \quad (\text{A26})$$

$$\lambda_{33} = - \frac{\omega_p^2}{\omega^2} \left[1 - \langle v_{\parallel}^2 \rangle \langle J_0^2 \frac{\partial}{\partial v_{\perp}} \rangle \right] + \frac{\omega_p^2}{\omega^2} \langle v_{\perp} J_0^2 \rangle \left(1 + \frac{\omega^2}{k_{\parallel}} \chi \right). \quad (\text{A27})$$

It is possible to get rid of the series in (A25)–(A27) using [21]

$$\Phi = \sum_{n \neq 0} \frac{J_n^2}{n^2} = \frac{4}{\pi} \int_0^{\pi/2} t^2 J_0(2x \cos t) dt - \frac{\pi^2}{6} J_0^2, \quad (\text{A28})$$

$$\Psi = \sum_{n \neq 0} \frac{J_n J'_n}{n^2} = \frac{1}{2} \frac{d\Phi}{dx}, \quad (\text{A29})$$

$$\Upsilon = \sum_{n \neq 0} \frac{(J'_n)^2}{n^2} = \frac{1}{2} \left[\frac{d^2\Phi}{dx^2} + \frac{1}{x} \frac{d\Phi}{dx} + 2\Phi - \frac{2}{x}(1 - J_0^2) \right]. \quad (\text{A30})$$

This may be useful for calculations in the regime $k_{\perp} v_{\perp} / \Omega \sim 1$.

The general dispersion relation is obtained from the determinant $\det |D| = 0$, where $D_{ij} = N^2 \delta_{ij} - N_i N_j - \epsilon_{ij}$, that is,

$$D_{11} = N_{\parallel}^2 - 1 - \sum \lambda_{11}, \quad (\text{A31})$$

$$D_{12} = - \sum \lambda_{12}, \quad (\text{A32})$$

$$D_{13} = -N_{\parallel} N_{\perp} - \sum \lambda_{13}, \quad (\text{A33})$$

$$D_{22} = N^2 - 1 - \sum \lambda_{22}, \quad (\text{A34})$$

$$D_{23} = - \sum \lambda_{23}, \quad (\text{A35})$$

$$D_{33} = N_{\perp}^2 - 1 - \sum \lambda_{33}. \quad (\text{A36})$$

The polarization should be found from the equations

$$D_{ij} E_j = 0. \quad (\text{A37})$$

Eq. (A37) provides the ratio of the electric field components. In order to translate that into the magnetic polarization one has to use the relation $\mathbf{B} = \mathbf{k} \times \mathbf{E} / \omega$. In order to find the density perturbations one has to use the current conservation as follows

$$\delta \rho = \mathbf{k} \cdot \mathbf{j} / \omega, \quad (\text{A38})$$

where

$$j_i = -i \frac{\omega}{4\pi} \lambda_{ij} E_j, \quad (\text{A39})$$

so that one has eventually

$$\delta \rho = -\frac{i}{4\pi} k_i \lambda_{ij} E_j. \quad (\text{A40})$$

Further simplifications are possible in the longwavelength limit.

APPENDIX B: LONGWAVELENGTH APPROXIMATION

In this appendix we provide general expressions for the dielectric tensor in the longwavelength limit $k_{\perp} v_{\perp} / \Omega \ll 1$, where $J_{\pm 1} = \pm k_{\perp} v_{\perp} / 2\Omega$, $J_0 = 1 - k_{\perp}^2 v_{\perp}^2 / 2\Omega^2$, and higher order Bessel functions may be neglected. In this limit one has

$$\lambda_{11} = \frac{\omega_p^2}{\Omega^2} + \frac{1}{2} N_{\parallel}^2 (\beta_{\parallel} - \beta_{\perp}), \quad (\text{B1})$$

$$\lambda_{12} = i \frac{\omega_p^2}{\omega \Omega}, \quad (\text{B2})$$

$$\lambda_{13} = -\frac{1}{2} N_{\parallel} N_{\perp} (\beta_{\parallel} - \beta_{\perp}), \quad (\text{B3})$$

$$\lambda_{22} = \frac{\omega_p^2}{\Omega^2} + \frac{1}{2} N_{\parallel}^2 (\beta_{\parallel} - \beta_{\perp}) \quad (\text{B4})$$

$$- N_{\perp}^2 \beta_{\perp} + \frac{N_{\perp}^2 \beta_{\perp}}{4} \frac{\langle v_{\perp}^4 \rangle}{\langle v_{\perp}^2 \rangle} \chi],$$

$$\lambda_{23} = i \frac{\beta_{\perp} \tan \theta \Omega}{2\omega} c^2 \chi, \quad (\text{B5})$$

$$\lambda_{33} = \frac{1}{2} N_{\perp}^2 (\beta_{\parallel} - \beta_{\perp}) + \left(\frac{\omega_p^2}{k_{\parallel}^2} - \frac{\beta_{\perp} \tan^2 \theta c^2}{2} \right) \chi, \quad (\text{B6})$$

where $N = kc/\omega$, $N_\perp = k_\perp c/\omega = N \sin \theta$, $N_\parallel = lk_\parallel c/\omega = N \cos \theta$, $\beta_\parallel = 2\omega_p^2 \langle v_\parallel^2 \rangle / c^2 \Omega^2$, $\beta_\perp = \omega_p^2 \langle v_\perp^2 \rangle / c^2 \Omega^2$, and $\langle \dots \rangle$ denotes usual averaging over the distribution. Here also $\zeta = u - v_\parallel$, where $u = \omega/k_\parallel$. The last term in (B6) is given for completeness. In the limit used in this paper, $\omega/\Omega \rightarrow 0$ and ω/k finite, it should be neglected. Throughout the paper we also assume $\omega_{pi} \gg \Omega_i$.

APPENDIX C: APERIODIC NATURE OF THE MIRROR INSTABILITY

In order to show that the mirror instability is aperiodic we analyze the behavior of the roots of (9) when the β parameters are changed. In the waterbag case the transition from the stable to the unstable regimes occurs when $W = 0, G = 0$ and for the mode whose phase velocity is less than the highest particle velocity, $\text{Re } Z < v_{\parallel, \text{max}}$ (“subparticle” mode), that is, in the resonant region. In the general case, where Landau damping is nonzero, in the resonant range every propagating wave having $W \neq 0$ has also nonzero damping rate $G < 0$ (we assume that there are no other kinetic instabilities in the mirror-stable region). By continuously changing the plasma parameters (e.g., the anisotropy ratio $\beta_\perp/\beta_\parallel$) we can bring the system into the unstable regime. Assuming continuous dependence of W and G on the plasma parameters we see that it is impossible for the “subparticle” mode with $W \neq 0$ to transform into the unstable mode, since $G < 0$ and cannot be made positive continuously. Thus, the only way to do that is to go through $W = 0, G = 0$.

Let us now consider the vicinity of the transition to the instability, $|Z| \ll 1$. In the most general way, expanding $\bar{\chi}$ in powers of Z one gets:

$$\begin{aligned} \bar{\chi} &= \int \frac{1}{Z - v_\parallel} \frac{\partial f}{\partial v_\perp} dv_\parallel \\ &= -\frac{1}{v_\parallel} \frac{\partial f}{\partial v_\perp} dv_\parallel + Z \int \frac{1}{Z - v_\parallel} \frac{1}{v_\parallel} \frac{\partial f}{\partial v_\perp} dv_\parallel \\ &\rightarrow d + i\kappa Z, \end{aligned} \tag{C1}$$

provided $(\partial f/\partial v_\parallel)|_{v_\parallel=0} \neq 0$. The quantities d and κ are defined in (14). It is easy to see that (9) is the first order equation for iZ (with real coefficients) in the lowest order on $|Z| \ll 1$, which means that there is a simple (one and only one) aperiodic root in the vicinity of $Z = 0$. Such aperiodic solutions cannot be converted into non-aperiodic ones by continuous change of the plasma parameters, for the same reason as above. Therefore, the unstable solutions must be aperiodic.

The function $\Psi(Z)$, defined in (9), is an analytical function of $Z = W + iG$ and a continuous function of its parameters β and θ . Let us consider how Z moves from the lower half-plane (stable regime) to the upper half-plane (unstable regime) with the change of β and $\theta = \text{const}$. The transition to instability occurs, in general, in the vicinity of $Z = 0$ where $\Psi(Z) = \Psi(0) + (d\Psi/dZ)|_{Z=0}Z = A + BZ$ (see sec. V). In the transition point $A = 0$. Using (15)–(17) it is easy to show that in the transition point $B > 0$ (provided $\kappa > 0$, this condition being violated if $\partial f/\partial \mathcal{E} > 0$ at $v_\parallel = 0$, corresponding to the regime of two-hump instability), so that in the vicinity of the transition point $A > 0$ corresponds to the stable regime, while $A < 0$ corresponds to the instability. Because of the continuity, in the whole instability range $A < 0$.

Let us show now that (9) always has a solution $Z = iG, G > 0$ in the unstable range. Indeed, $\Psi(0) < 0$ as is shown above. On the other hand, if $G \rightarrow \infty$ one has $\chi \rightarrow 1/G^2$ and $\Psi(\infty) > 0$. This means that there exists $G > 0$ such that $\Psi(G) = 0$.

In the absence of kinetic instabilities, in the stable regime all roots of (9) with nonzero W are either in the lower half-plane (Landau damping or nonpropagation) or at the real axis (if $(\partial f/\partial v_\parallel)|_{v_\parallel=W} = 0$). In the first case no root can cross the real axis except at $W = 0$, when the parameters are changed continuously to bring the system in the unstable regime. As can be seen from (15)–(17) there is only one root crossing the real axis at this point, provided $\partial f/\partial \mathcal{E} < 0$. Therefore, there is only one root in the upper half-plane and it is purely imaginary.

If $\partial f/\partial \mathcal{E} = 0$ there are two or more roots in the vicinity of $Z = 0$ (depending on the behavior of f) but only one is positive, $G > 0$. Since in this case the analytical continuation through $Z = 0$ into the lower half-plane is straightforward (no pole at $v_\parallel = 0$) other roots correspond to damping solutions, and there is again only one root in the upper half-plane.

Finally, let us consider the case where there are roots with $G = 0$ and $W = W_0 \neq 0$. Such situation can occur when $(\partial f/\partial v_\parallel) = 0$ in isolated points or in an interval (as for the compact waterbag and hard-bell). In the first case the imaginary part of Z is negative for W close to W_0 , so that the continuous change of parameters does not bring the root to the upper half-plane.

In the second case the continuous change of parameters leaves the root on the real axis until it enters the range where $(\partial f/\partial v_\parallel) \neq 0$ or $W = 0$.

[1] Krauss-Varban, D., Omidi, N., and Quest, K.B., Mode properties of low-frequency waves: Kinetic theory versus Hall-MHD, J. Geophys. Res., 99, 5987, 1994.

- [2] D. S. Orłowski, C. T. Russell, D. Krauss-Varban, and N. Omid, A test of the Hall-MHD model: Application to low-frequency upstream waves at Venus, *J. Geophys. Res.*, **99**, 169-178, 1994.
- [3] Kaufmann, R.L., Horng, J.T., and Wolfe, A., Large-amplitude hydromagnetic waves in inner magnetosheath, *J. Geophys. Res.*, **75**, 4666, 1970.
- [4] Tsurutani, B.T., Smith, E.J., Anderson, R.R., Ogilvie, K.W., Scudder, J.D., Baker, D.N., and Bame, S.J., Lion roars and nonoscillatory drift mirror waves in the magnetosheath, *J. Geophys. Res.*, **87**, 6060, 1982.
- [5] Violante, L., Bavassano-Cattaneo, B., Moreno, G., and Richardson, J.D., Observations of mirror waves and plasma depletion layer upstream of Saturn's magnetopause, *J. Geophys. Res.*, **100**, 12047, 1995.
- [6] Czaykowska, A., Bauer, T.M., Treumann, R.A., and Baumjohann, W., Mirror waves downstream of the quasi-perpendicular bow shock, *J. Geophys. Res.*, **103**, 4747, 1998.
- [7] Winterhalter, D., Neugebauer, M., Goldstein, B.E., Smith, E.J., Bame, S.J., and Balogh, A., Ulysses field and plasma observations of magnetic holes in the solar wind and their relation to mirror-mode structures, *J. Geophys. Res.*, **99**, 23,371, 1994.
- [8] Russell, C.T., Riedler, W., Schwingenschuch, K., and Yeroshenko, Y., Mirror instability in the magnetosphere of comet Halley, *Geophys. Res. Lett.*, **14**, 644, 1987.
- [9] Vaisberg, O.L., Russell, C.T., Luhmann, J.G., and Schwingenschuch, K., Small-scale irregularities in comet Halley's plasma mantle: An attempt at self-consistent analysis of plasma and magnetic field data, *Geophys. Res. Lett.*, **16**, 5, 1989.
- [10] Kivelson, M.G., Khurana, K.K., Walker, R.J., Warnecke, J., Russell, C.T., Linker, J.A., Southwood, D.J., and Polansky, C., Io's interaction with the plasma Torus: Galileo magnetometer report, *Science*, **274**, 396, 1996.
- [11] Russell, C.T., Huddleston, D.E., Strangeway, R.J., Blanco-Cano, X., Kivelson, M.G., Khurana, K.K., Frank, L.A., Paterson, W., Gurnett, D.A., and Kurth, W.S., Mirror-mode structures at the Galileo-Io flyby: Observations, *J. Geophys. Res.*, **104**, 17,471, 1999.
- [12] Hasegawa, A., *Plasma instabilities and nonlinear effects*, Springer-Verlag, New York, 1975.
- [13] Gary, S.P., The mirror and ion cyclotron anisotropy instabilities, *J. Geophys. Res.*, **97**, 8519, 1992.
- [14] McKean, M.E., Winske, D., and Gary, S.P., Mirror and ion cyclotron anisotropy instabilities in the magnetosheath, *J. Geophys. Res.*, **97**, 19,421, 1992.
- [15] Gary, S.P., Fuselier, S.A., and Anderson, B.J., Ion anisotropy instabilities in the magnetosheath, *J. Geophys. Res.*, **98**, 1481, 1993.
- [16] Southwood, D.J., and Kivelson, M.G., Mirror instability, 1, Physical mechanism of linear stability, *J. Geophys. Res.*, **98**, 9181, 1993.
- [17] Pantellini, F.G.E., and Schwartz, S.J., Electron temperature effects in the linear proton mirror instability, *J. Geophys. Res.*, **100**, 3539, 1995.
- [18] Pokhotelov, O.A., Balikhin, M.A., Alleyne, H.S.C.K., Onishchenko, O.G., Mirror instability with finite electron temperature effects, *J. Geophys. Res.*, **105**, 2393, 2000.
- [19] Kivelson, M.G., and Southwood, D.J., Mirror instability, 2, The mechanism of nonlinear saturation, *J. Geophys. Res.*, **101**, 17,365, 1996.
- [20] Sckopke, N., Paschmann, G., Brinca, A.L., Carlson, C.W., and Luhr, H., Ion thermalizations in quasi-perpendicular shocks involving reflected ions, *J. Geophys. Res.*, **95**, 6337, 1990.
- [21] Prudnikov, A.P., Brychkov, Yu. A., and Marichev, O.I., *Integrals and series*, New York : Gordon and Breach Science Publishers, 1988.

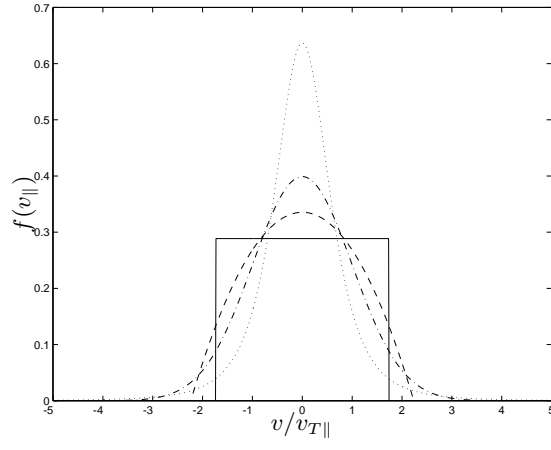


FIG. 1: Waterbag (solid line), hard bell (dashed), Lorentz (dotted), and Maxwellian (dash-dotted) distributions.

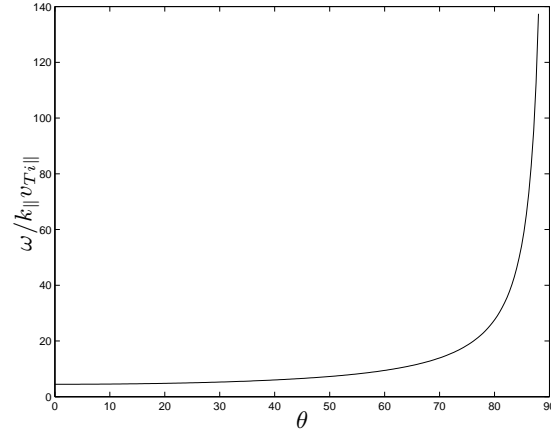


FIG. 2: Phase velocity of the fast mode as a function of propagation angle for the case of the waterbag distribution with $\beta_{i\parallel} = \beta_{i\perp} = \beta_{e\parallel} = \beta_{e\perp} = 0.1$ and massless bi-Maxwellian electrons.

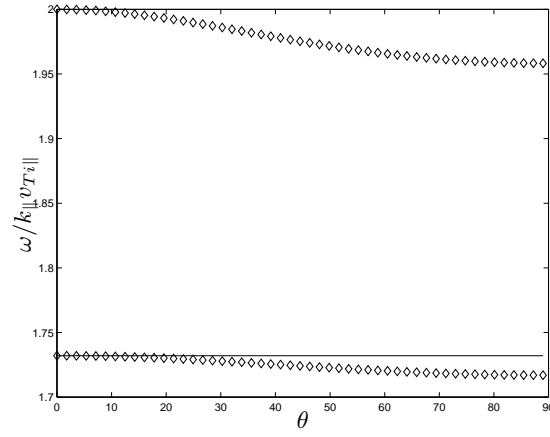


FIG. 3: Phase velocity (diamonds) of the two low-velocity modes as a function of propagation angle for the case of the waterbag distribution with $\beta_{i\parallel} = \beta_{i\perp} = \beta_{e\parallel} = \beta_{e\perp} = 0.1$ and massless bi-Maxwellian electrons. The solid line is $\omega = \sqrt{a_i} k_{\parallel} v_{Ti\parallel} = k_{\parallel} v_{0i}$.

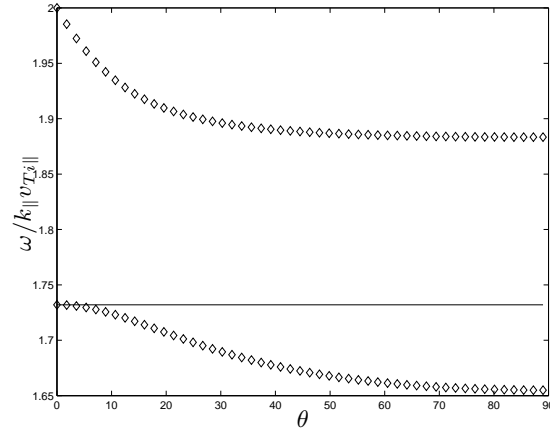


FIG. 4: Phase velocity (diamonds) of the two low-velocity modes as a function of propagation angle for the case of the waterbag distribution with $\beta_{i\parallel} = \beta_{i\perp} = \beta_{e\parallel} = \beta_{e\perp} = 0.5$ and massless bi-Maxwellian electrons. The solid line is $\omega = \sqrt{a_i} k_{\parallel} v_{Ti\parallel} = k_{\parallel} v_{0i}$.

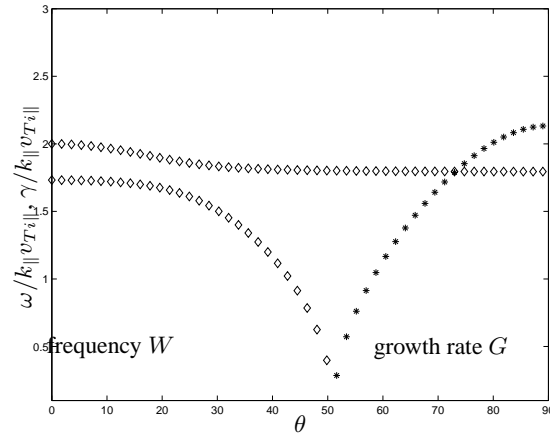


FIG. 5: Behavior of the two low-velocity modes as a function of propagation angle for the case of the waterbag distribution with $\beta_{i\parallel} = \beta_{e\parallel} = 0.1$, $\beta_{i\perp} = \beta_{e\perp} = 0.5$ (so that $K = 1$), and massless bi-Maxwellian electrons. Diamonds mark the modes in the range where their frequencies are purely real, stars show the growth rate of the aperiodic instability.

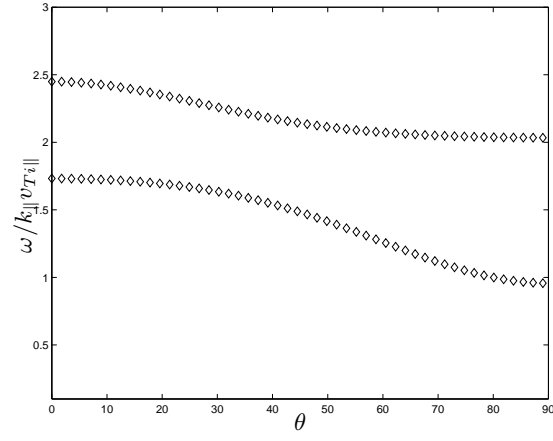


FIG. 6: Behavior of the two low-velocity modes as a function of propagation angle for the case of the waterbag distribution with $\beta_{i||} = \beta_{e||} = 0.1$, $\beta_{i\perp} = \beta_{e\perp} = 0.5$ (so that $K = 1$), and waterbag electrons, $d_e = 1/3$. There is no instability.

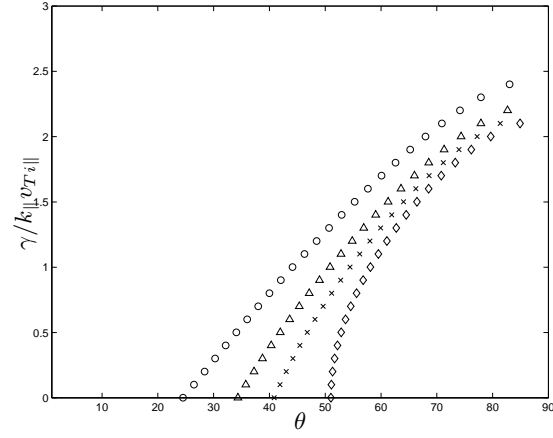


FIG. 7: Growth rates for the mirror instability in the case of $\beta_{i||} = \beta_{e||} = 0.1$, $\beta_{i\perp} = \beta_{e\perp} = 0.5$, and massless bi-Maxwellian electrons $d_e = 1$, and four different distributions: waterbag (diamonds), hard-bell (crosses), Lorentz (circles), and bi-Maxwellian (triangles).

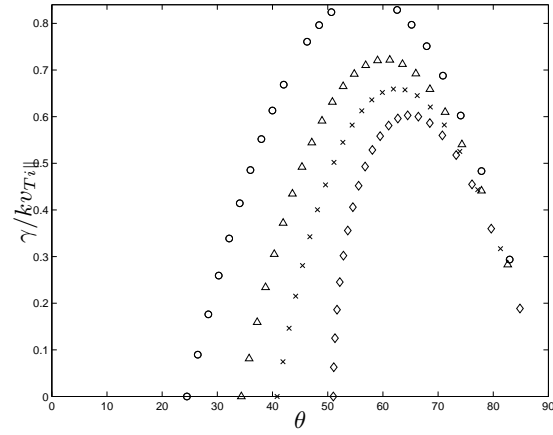


FIG. 8: Growth rates for the mirror instability in the case of $\beta_{i||} = \beta_{e||} = 0.1$, $\beta_{i\perp} = \beta_{e\perp} = 0.5$, and massless bi-Maxwellian electrons $d_e = 1$, and four different distributions: waterbag (diamonds), hard-bell (crosses), Lorentz (circles), and bi-Maxwellian (triangles), normalized on $k v_{Te||}$.

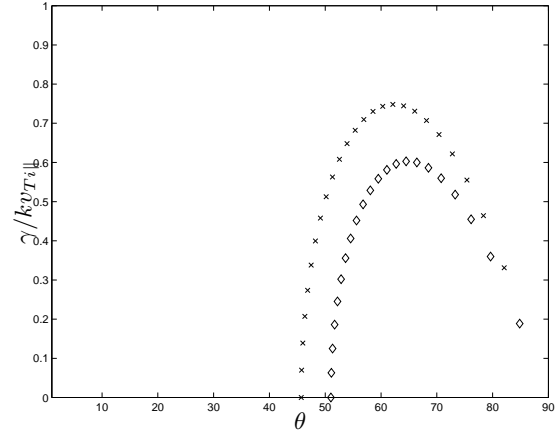


FIG. 9: Dependence of the growth rate on β_{\perp} with $K = 1$ for waterbag ions and massless bi-Maxwellian electrons: diamonds correspond to $\beta_{i\parallel} = \beta_{e\parallel} = 0.1, \beta_{i\perp} = \beta_{e\perp} = 0.5$, crosses correspond to $\beta_{i\parallel} = \beta_{e\parallel} = 0.25, \beta_{i\perp} = \beta_{e\perp} = 1$.

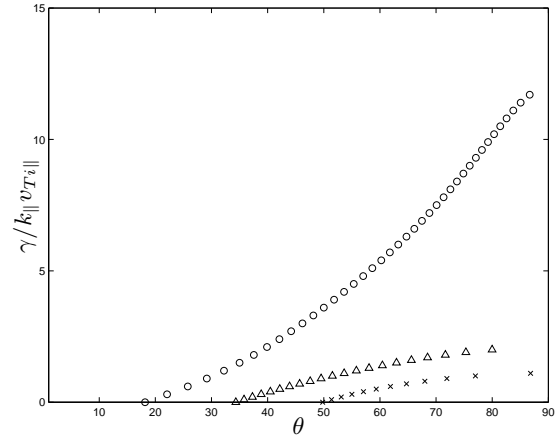


FIG. 10: Growth rates for the mirror instability in the case of $\beta_{i\parallel} = \beta_{e\parallel} = 0.1, \beta_{i\perp} = \beta_{e\perp} = 0.5$, and three different combinations: hard-bell ions and electrons (crosses), Lorentz ions and electrons (circles), and bi-Maxwellian ions and (massive) electrons (triangles).

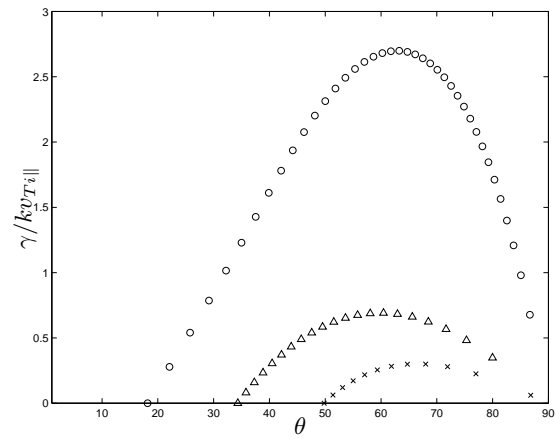


FIG. 11: Same as in Figure 10 but normalized on $kv_{Ti\parallel}$.

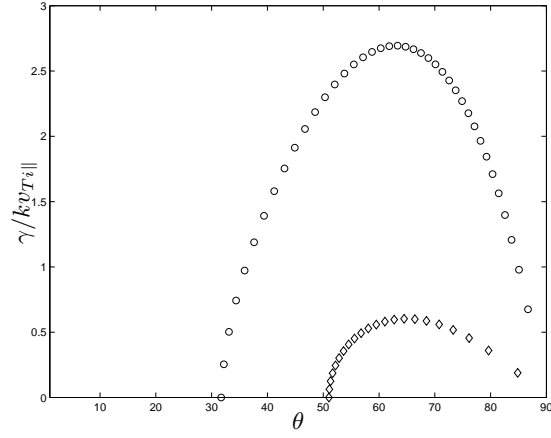


FIG. 12: Growth rates for the mirror instability in the case of $\beta_{i\parallel} = \beta_{e\parallel} = 0.1$, $\beta_{i\perp} = \beta_{e\perp} = 0.5$, waterbag ions and two different electron distributions: massive bi-Maxwellian (diamonds) and Lorentz (circles).

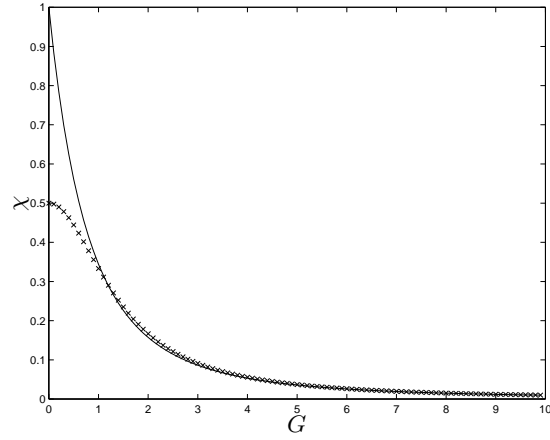


FIG. 13: Approximation of $\chi(G)$ for the Maxwellian distribution. The numerically calculated $\chi(G)$ (solid line) is compared to $\chi = (G^2 + 2)^{-1}$ (crosses).

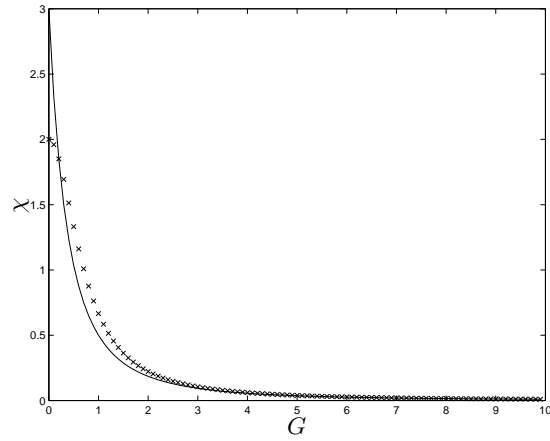


FIG. 14: Approximation of $\chi(G)$ for the Lorentzian distribution. The numerically calculated $\chi(G)$ (solid line) is compared to $\chi = (G^2 + 0.5)^{-1}$ (crosses).

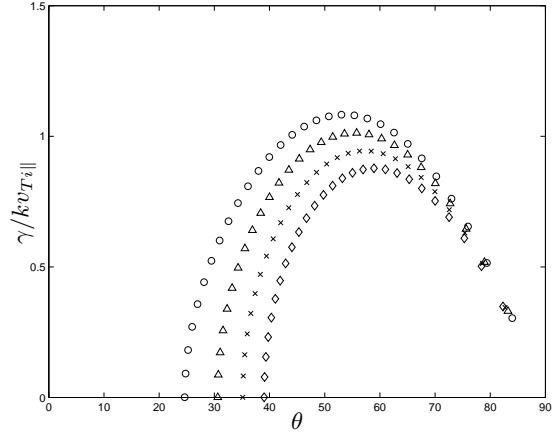


FIG. 15: Growth rates for the mirror instability in the case of $\beta_{i\parallel} = \beta_{e\parallel} = 0.1$, $\beta_{i\perp} = \beta_{e\perp} = 0.5$, calculated with the approximation $\bar{\chi}_i = 1/(G^2 + v_m^2)$, for several $v_m^2 = 2$ (diamonds), 1.5 (crosses), 1 (triangles), and 0.5 (circles). The electrons are massless Maxwellian.

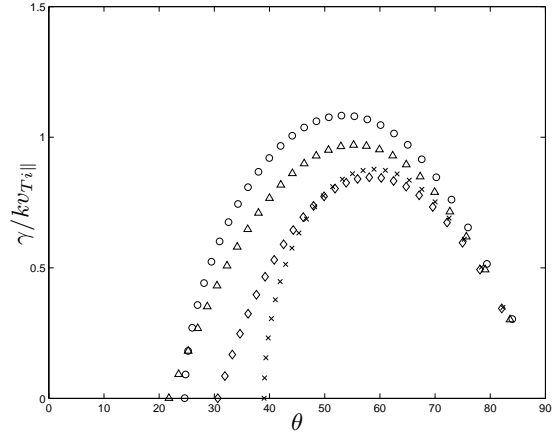


FIG. 16: Comparison of the growth rates for the mirror instability in the case of $\beta_{i\parallel} = \beta_{e\parallel} = 0.1$, $\beta_{i\perp} = \beta_{e\perp} = 0.5$, calculated directly and with the approximation $\bar{\chi}_i = 1/(G^2 + v_m^2)$, for Maxwellian (diamonds and crosses, respectively) and Lorentzian (triangles and circles, respectively). The electrons are massless Maxwellian.